# Summary of the Abrahamson & Silva NGA Ground-Motion Relations

**Norman Abrahamson,[a) M.EERI,** and **Walter Silva,[b) M.EERI**

Empirical ground-motion models for the rotation-independent average horizontal component from shallow crustal earthquakes are derived using the PEER NGA database. The model is applicable to magnitudes 5–8.5, distances $0-200$ km, and spectral periods of $0-10$ sec. In place of generic site categories (soil and rock), the site is parameterized by average shear-wave velocity in the top 30 m ($V_{S30}$) and the depth to engineering rock (depth to $V_S = 1000$ m/s). In addition to magnitude and style-of-faulting, the source term is also dependent on the depth to top-of-rupture: for the same magnitude and rupture distance, buried ruptures lead to larger short-period ground motions than surface ruptures. The hanging-wall effect is included with an improved model that varies smoothly as a function of the source properties (M, dip, depth), and the site location. The standard deviation is magnitude dependent with smaller magnitudes leading to larger standard deviations. The short-period standard deviation model for soil sites is also distant-dependent due to nonlinear site response, with smaller standard deviations at short distances. [DOI: 10.1193/1.2924360]

## INTRODUCTION

In previous ground-motion models, the range of applicability of the empirical ground-motion models was based on the range covered by the available empirical data set; however, in hazard studies, the ground motion must be computed for all relevant earthquakes, so the limits on the range of applicability were often ignored. To address this issue, the Next Generation Attenuation (NGA) project required the developers of the models to extrapolate their models such that they are applicable to all crustal earthquakes relevant for seismic hazard analyses in California: M5–M8.5 for strike-slip, M5–M8.0 for dip-slip, distance $0-200$ km, and spectral periods up to 10 seconds.

A recurring comment on the NGA project is that the empirical data is not adequate to constrain the ground motion over the entire specified range. The concept behind the NGA project is that the developers are better suited to extrapolate their models for application outside the range well constrained by the empirical data than the hazard analyst. To support the developers in this extrapolation, the NGA project used three classes of analytical models to provide the developers with constraints on the ground-motion scaling outside the range well constrained by the empirical data. These analytical models included hard-rock ground motions based on 1-D finite-fault kinematic source models

a) Pacific Gas & Electric Company, 245 Market Street, San Francisco, CA 94105
b) Pacific Engineering and Analysis, 311 Pomona Ave., El Cerrito, CA 94546

for M6.5 to M8.25 (Collins et al. 2006), 3-D basin response simulations for sites in southern California (Day et al. 2006), and equivalent-linear site response simulations (Walling et al. 2008).

The development of the NGA models is not simple curve fitting, but rather, it is model building that uses seismological and geotechnical information, in addition to the empirical ground-motion data, to develop the models. The NGA models are intended to begin the transition from simple empirical models to full numerical simulations for specific source-site geometries.

In this paper, we summarize our NGA model. We have made extensive use of the results from the analytical models to constrain the scaling in our empirical ground motion model. Complete descriptions of the basis for the selection of the data set, the basis for the functional form of the ground-motion model, the details of the regression analysis, and a comprehensive set of residual plots are given in Abrahamson and Silva (2008).

## DATA SET SELECTION

We selected our ground-motion data set from the NGA data base (flat-file version 7.2). Our general approach for selecting the subset of data for use in the regression analysis was to include all earthquakes, including aftershocks, from shallow crustal earthquakes in active tectonic regions under the assumption that the median ground motions from shallow crustal earthquakes at distances less than about 100 km are similar around the world. In particular, we included the Chi-Chi mainshock, Chi-Chi aftershocks, Kocaeli mainshock, and Duzce aftershock.

In the context of simple source models, we are assuming that median stress-drops are similar among different active tectonic regions with shallow crustal earthquakes (e.g., California, Alaska, Taiwan, Japan, Turkey, Italy, Greece, New Zealand, Northwest China). We tested the validity of this assumption by comparing the inter-event residuals from earthquakes in other regions with those from earthquakes in California (Abrahamson and Silva 2008).

At distances greater than 100 km, differences in crustal structure can have significant effects on the ground motion leading to a change in the attenuation at large distances (e.g., Q term). Since the objective of this study is to develop ground motion models applicable to California, we excluded recordings at distances greater than 100 km from earthquakes outside of the western U.S. (WUS).

A summary of the criteria for excluding earthquakes and recordings is given below:
- Remove earthquakes not representative of shallow crustal tectonics
- Remove earthquakes missing key source meta data
- Remove recordings not representative of free-field ground motion
- Remove recordings without a $V_{S30}$ estimate
- Remove duplicate recordings from co-located stations
- Remove recordings with missing horizontal components or poor quality accelerograms

- Remove non-WUS recordings at rupture distances greater than 100 km
- Remove WUS recordings at rupture distances greater than 200 km

Our data set consists of 2754 recordings from 135 earthquakes. The earthquakes used in our analysis are listed in Table 1. Events not in the WUS are listed as "Other" for the event region. The NGA flat-file did not include an event class (Table 1) so we assigned the event classes. The classifications are not all unambiguous. For example, we classified the 1999 Ducze earthquake (EQID 138) as an aftershock of the 1999 Kocaeli earthquake since its rupture overlapped part of the Kocaeli rupture and it occurred shortly after the Kocaeli mainshock; however, this event could also have been considered to be a triggered event and classified as a mainshock since most of the rupture is on an adjacent segment of the North Anatolian fault. Since the ground motion from Duzce is lower than average for mainshocks, classifying this event as a mainshock would lead to a reduction in the median ground motion for mainshocks and an increase in the inter-event standard deviation as compared to classifying it as an aftershock.

The response spectral values for the selected recordings are only used in the regression analysis for spectral frequencies greater than 1.25 times the high-pass corner frequency used in the record processing, as defined in the NGA database. This requirement produces a data set that varies as a function of period. For example, at a period of 5 seconds, the data set is reduced to 987 recordings from 64 earthquakes. The period dependence of the number of earthquakes and number of recordings used in the regression analysis is shown in Figure 1.

## SITE CLASSIFICATION

The site condition is classified using two parameters: the average shear-wave velocity in the top 30 m ($V_{S30}$) and the depth to $V_S=1.0$ km/s ($Z_{1.0}$). Using $V_{S30}$ in place of generic soil and rock categories has the advantage that it is consistent with the site classification used in current building codes. This does not imply that 30 m is the key depth range for the site response, but rather that $V_{S30}$ is correlated with the entire soil profile. Using the soil depth in addition to $V_{S30}$ allows the ground-motion model to distinguish between shallow soil sites, average depth soil sites, and deep soil sites.

## DISTANCE DEFINITION

In previous studies, several different distance definitions have been used for developing attenuation relations. In this study, we use the closest distance to the rupture plane, $R_{rup}$, as the primary distance measure. Two additional distance measures, $R_{JB}$ and $R_x$ are used to model the attenuation of hanging wall effects: $R_{JB}$ is the closest horizontal distance to the surface projection of the rupture; $R_x$ is the horizontal distance from the top edge of the rupture, measured perpendicular to the fault strike. The magnitude-distance distributions for PGA and T=5 sec are shown in Figure 2.

**Table 1.** Summary of selected earthquakes

| EQID | YEAR | Earthquake Name | Mag | Number of Recordings | Event Class | Event Region |
|------|------|-----------------|-----|---------------------|-------------|--------------|
| 12 | 1952 | Kern County | 7.36 | 1 | MS | CA |
| 20 | 1957 | San Francisco | 5.28 | 1 | MS | CA |
| 25 | 1966 | Parkfield | 6.19 | 4 | MS | CA |
| 28 | 1968 | Borrego Mtn | 6.63 | 1 | MS | CA |
| 29 | 1970 | Lytle Creek | 5.33 | 10 | MS | CA |
| 30 | 1971 | San Fernando | 6.61 | 35 | MS | CA |
| 31 | 1972 | Managua, Nicaragua-01 | 6.24 | 1 | MS | Other |
| 32 | 1972 | Managua, Nicaragua-02 | 5.2 | 1 | AS | Other |
| 33 | 1973 | Point Mugu | 5.65 | 1 | MS | CA |
| 34 | 1974 | Hollister-03 | 5.14 | 2 | MS | CA |
| 35 | 1975 | Northern Calif-07 | 5.2 | 5 | MS | CA |
| 36 | 1975 | Oroville-01 | 5.89 | 1 | MS | CA |
| 37 | 1975 | Oroville-02 | 4.79 | 2 | AS | CA |
| 38 | 1975 | Oroville-04 | 4.37 | 3 | AS | CA |
| 39 | 1975 | Oroville-03 | 4.70 | 9 | AS | CA |
| 40 | 1976 | Friuli, Italy-01 | 6.5 | 4 | MS | Other |
| 41 | 1976 | Gazli, USSR | 6.8 | 1 | MS | Other |
| 42 | 1976 | Fruili, Italy-03 | 5.5 | 3 | AS | Other |
| 43 | 1976 | Friuli, Italy-02 | 5.91 | 4 | AS | Other |
| 45 | 1978 | Santa Barbara | 5.92 | 1 | MS | CA |
| 46 | 1978 | Tabas, Iran | 7.35 | 4 | MS | Other |
| 47 | 1979 | Dursunbey, Turkey | 5.34 | 1 | MS | Other |
| 48 | 1979 | Coyote Lake | 5.74 | 10 | MS | CA |
| 49 | 1979 | Norcia, Italy | 5.9 | 2 | MS | Other |
| 50 | 1979 | Imperial Valley-06 | 6.53 | 33 | MS | CA |
| 51 | 1979 | Imperial Valley-07 | 5.01 | 16 | AS | CA |
| 52 | 1979 | Imperial Valley-08 | 5.62 | 1 | AS | CA |
| 53 | 1980 | Livermore-01 | 5.8 | 6 | MS | CA |
| 54 | 1980 | Livermore-02 | 5.42 | 7 | AS | CA |
| 55 | 1980 | Anza (Horse Canyon)-01 | 5.19 | 5 | MS | CA |
| 56 | 1980 | Mammoth Lakes-01 | 6.06 | 3 | Swarm | CA |
| 57 | 1980 | Mammoth Lakes-02 | 5.69 | 3 | Swarm | CA |
| 58 | 1980 | Mammoth Lakes-03 | 5.91 | 4 | Swarm | CA |
| 59 | 1980 | Mammoth Lakes-04 | 5.7 | 3 | Swarm | CA |
| 60 | 1980 | Mammoth Lakes-05 | 5.7 | 2 | Swarm | CA |
| 61 | 1980 | Mammoth Lakes-06 | 5.94 | 5 | Swarm | CA |
| 62 | 1980 | Mammoth Lakes-07 | 4.73 | 6 | AS | CA |
| 63 | 1980 | Mammoth Lakes-08 | 4.8 | 7 | AS | CA |
| 64 | 1980 | Victoria, Mexico | 6.33 | 4 | MS | CA |
| 65 | 1980 | Mammoth Lakes-09 | 4.85 | 9 | AS | CA |
| 68 | 1980 | Irpinia, Italy-01 | 6.9 | 12 | MS | Other |
| 69 | 1980 | Irpinia, Italy-02 | 6.2 | 10 | AS | Other |

**Table 1.** (**cont.**)

| EQID | YEAR | Earthquake Name | Mag | Number of Recordings | Event Class | Event Region |
|------|------|-----------------|-----|----------------------|-------------|--------------|
| 70 | 1981 | Irpinia, Italy-03 | 4.70 | 1 | AS | Other |
| 71 | 1981 | Taiwan SMART1(5) | 5.9 | 7 | MS | Other |
| 72 | 1981 | Corinth, Greece | 6.6 | 1 | MS | Other |
| 73 | 1981 | Westmorland | 5.9 | 6 | MS | CA |
| 74 | 1983 | Mammoth Lakes-10 | 5.34 | 1 | AS | CA |
| 75 | 1983 | Mammoth Lakes-11 | 5.31 | 1 | AS | CA |
| 76 | 1983 | Coalinga-01 | 6.36 | 45 | MS | CA |
| 77 | 1983 | Coalinga-02 | 5.09 | 20 | AS | CA |
| 78 | 1983 | Coalinga-03 | 5.38 | 3 | AS | CA |
| 79 | 1983 | Coalinga-04 | 5.18 | 11 | AS | CA |
| 80 | 1983 | Coalinga-05 | 5.77 | 9 | AS | CA |
| 81 | 1983 | Coalinga-06 | 4.89 | 2 | AS | CA |
| 82 | 1983 | Coalinga-07 | 5.21 | 2 | AS | CA |
| 83 | 1983 | Ierissos, Greece | 6.7 | 1 | MS | Other |
| 84 | 1983 | Trinidad offshore | 5.7 | 2 | MS | CA |
| 85 | 1983 | Coalinga-08 | 5.23 | 2 | AS | CA |
| 86 | 1983 | Taiwan SMART1(25) | 6.5 | 9 | MS | Other |
| 87 | 1983 | Borah Peak, ID-01 | 6.88 | 2 | MS | WUS |
| 88 | 1983 | Borah Peak, ID-02 | 5.1 | 3 | AS | WUS |
| 90 | 1984 | Morgan Hill | 6.19 | 27 | MS | CA |
| 91 | 1984 | Lazio-Abruzzo, Italy | 5.8 | 5 | MS | Other |
| 94 | 1984 | Bishop (Rnd Val) | 5.82 | 1 | MS | CA |
| 95 | 1985 | Taiwan SMART1(33) | 5.8 | 7 | MS | Other |
| 96 | 1985 | Drama, Greece | 5.2 | 1 | MS | Other |
| 97 | 1985 | Nahanni, Canada | 6.76 | 3 | MS | Other |
| 98 | 1986 | Hollister-04 | 5.45 | 3 | MS | CA |
| 99 | 1986 | Mt. Lewis | 5.6 | 1 | MS | CA |
| 100 | 1986 | Taiwan SMART1(40) | 6.32 | 8 | MS | Other |
| 101 | 1986 | N. Palm Springs | 6.06 | 32 | MS | CA |
| 102 | 1986 | Chalfant Valley-01 | 5.77 | 5 | FS | CA |
| 103 | 1986 | Chalfant Valley-02 | 6.19 | 11 | MS | CA |
| 104 | 1986 | Chalfant Valley-03 | 5.65 | 3 | AS | CA |
| 105 | 1986 | Chalfant Valley-04 | 5.44 | 2 | AS | CA |
| 108 | 1986 | San Salvador | 5.8 | 2 | MS | Other |
| 111 | 1987 | New Zealand-02 | 6.6 | 2 | MS | Other |
| 113 | 1987 | Whittier Narrows-01 | 5.99 | 108 | MS | CA |
| 114 | 1987 | Whittier Narrows-02 | 5.27 | 9 | AS | CA |
| 115 | 1987 | Superstition Hills-01 | 6.22 | 1 | FS | CA |
| 116 | 1987 | Superstition Hills-02 | 6.54 | 11 | MS | CA |
| 117 | 1988 | Spitak, Armenia | 6.77 | 1 | MS | Other |
| 118 | 1989 | Loma Prieta | 6.93 | 77 | MS | CA |
| 119 | 1990 | Griva, Greece | 6.1 | 1 | MS | Other |

**Table 1.** (**cont.**)

| EQID | YEAR | Earthquake Name | Mag | Number of Recordings | Event Class | Event Region |
|------|------|-----------------|-----|------------------------|-------------|--------------|
| 120 | 1991 | Georgia, USSR | 6.2 | 5 | MS | Other |
| 121 | 1992 | Erzican, Turkey | 6.69 | 1 | MS | Other |
| 122 | 1992 | Roermond, Netherlands | 5.3 | 2 | MS | Other |
| 123 | 1992 | Cape Mendocino | 7.01 | 6 | MS | CA |
| 125 | 1992 | Landers | 7.28 | 68 | MS | CA |
| 126 | 1992 | Big Bear-01 | 6.46 | 38 | MS | CA |
| 127 | 1994 | Northridge-01 | 6.69 | 155 | MS | CA |
| 128 | 1994 | Double Springs | 5.9 | 1 | MS | CA |
| 129 | 1995 | Kobe, Japan | 6.9 | 20 | MS | Other |
| 130 | 1995 | Kozani, Greece-01 | 6.4 | 3 | MS | Other |
| 131 | 1995 | Kozani, Greece-02 | 5.1 | 2 | AS | Other |
| 132 | 1995 | Kozani, Greece-03 | 5.3 | 2 | AS | Other |
| 133 | 1995 | Kozani, Greece-04 | 5.1 | 2 | AS | Other |
| 134 | 1995 | Dinar, Turkey | 6.4 | 2 | MS | Other |
| 136 | 1999 | Kocaeli, Turkey | 7.51 | 17 | MS | Other |
| 137 | 1999 | Chi-Chi, Taiwan | 7.62 | 318 | MS | Other |
| 138 | 1999 | Duzce, Turkey | 7.14 | 13 | AS | Other |
| 139 | 1972 | Stone Canyon | 4.81 | 3 | MS | CA |
| 140 | 1972 | Sitka, Alaska | 7.68 | 1 | MS | WUS |
| 141 | 1976 | Caldiran, Turkey | 7.21 | 1 | MS | Other |
| 143 | 1990 | Upland | 5.63 | 3 | MS | CA |
| 144 | 1990 | Manjil, Iran | 7.37 | 5 | MS | Other |
| 145 | 1991 | Sierra Madre | 5.61 | 9 | MS | CA |
| 147 | 1994 | Northridge-02 | 6.05 | 15 | AS | CA |
| 148 | 1994 | Northridge-03 | 5.2 | 7 | AS | CA |
| 149 | 1994 | Northridge-04 | 5.93 | 7 | AS | CA |
| 150 | 1994 | Northridge-05 | 5.13 | 8 | AS | CA |
| 151 | 1994 | Northridge-06 | 5.28 | 48 | AS | CA |
| 152 | 1992 | Little Skull Mtn,NV | 5.65 | 8 | MS | CA |
| 153 | 1997 | Northwest China-01 | 5.9 | 2 | Swarm | Other |
| 154 | 1997 | Northwest China-02 | 5.93 | 2 | Swarm | Other |
| 155 | 1997 | Northwest China-03 | 6.1 | 1 | Swarm | Other |
| 156 | 1997 | Northwest China-04 | 5.8 | 2 | Swarm | Other |
| 157 | 1998 | San Juan Bautista | 5.17 | 1 | MS | CA |
| 158 | 1999 | Hector Mine | 7.13 | 79 | MS | CA |
| 160 | 2000 | Yountville | 5.0 | 24 | MS | CA |
| 161 | 2001 | Big Bear | 4.53 | 42 | MS | CA |
| 162 | 2001 | Mohawk Val, Portola | 5.17 | 6 | MS | CA |
| 163 | 2001 | Anza-02 | 4.92 | 72 | MS | CA |
| 164 | 2001 | Gulf of California | 5.7 | 11 | MS | CA |
| 165 | 2002 | CA-Baja Border Area | 5.31 | 9 | MS | CA |

**Table 1.** (**cont.**)

| EQID | YEAR | Earthquake Name | Mag | Number of Recordings | Event Class | Event Region |
|------|------|-----------------|-----|----------------------|-------------|--------------|
| 166 | 2002 | Gilroy | 4.9 | 34 | MS | CA |
| 167 | 2002 | Yorba Linda | 4.27 | 12 | MS | CA |
| 168 | 2002 | Nenana Mountain, Alaska | 6.7 | 5 | FS | WUS |
| 169 | 2002 | Denali, Alaska | 7.9 | 9 | MS | WUS |
| 170 | 2003 | Big Bear City | 4.92 | 35 | MS | CA |
| 171 | 1999 | Chi-Chi, Taiwan-02 | 5.9 | 195 | AS | Other |
| 172 | 1999 | Chi-Chi, Taiwan-03 | 6.2 | 189 | AS | Other |
| 173 | 1999 | Chi-Chi, Taiwan-04 | 6.2 | 202 | AS | Other |
| 174 | 1999 | Chi-Chi, Taiwan-05 | 6.2 | 166 | AS | Other |
| 175 | 1999 | Chi-Chi, Taiwan-06 | 6.3 | 188 | AS | Other |

[*]AS=aftershocks, MS=mainshocks, FS=foreshocks

## FUNCTIONAL FORM OF THE MODEL

The development of the functional form for our ground-motion model is described in detail in Abrahamson and Silva (2008). There are five key changes to the functional form as compared to our previous model (Abrahamson and Silva 1997): (1) $V_{S30}$ is used in place of generic soil and rock categories and the $V_{S30}$ dependence of the nonlinear site response effects are included; (2) the effect of soil depth is included for long periods; (3) the model distinguishes between buried and surface ruptures; (4) the hanging-
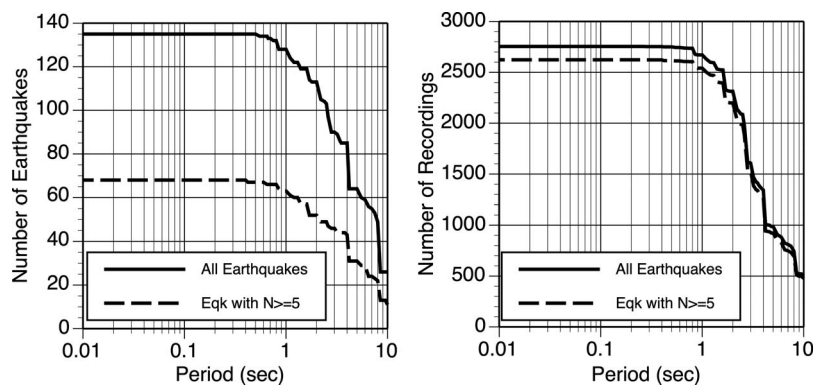


**Figure 1.** Period dependence of the number of earthquakes in our subset based on the lowest usable frequency for the average horizontal component listed in the flat-file. N is the number of recordings per earthquake.
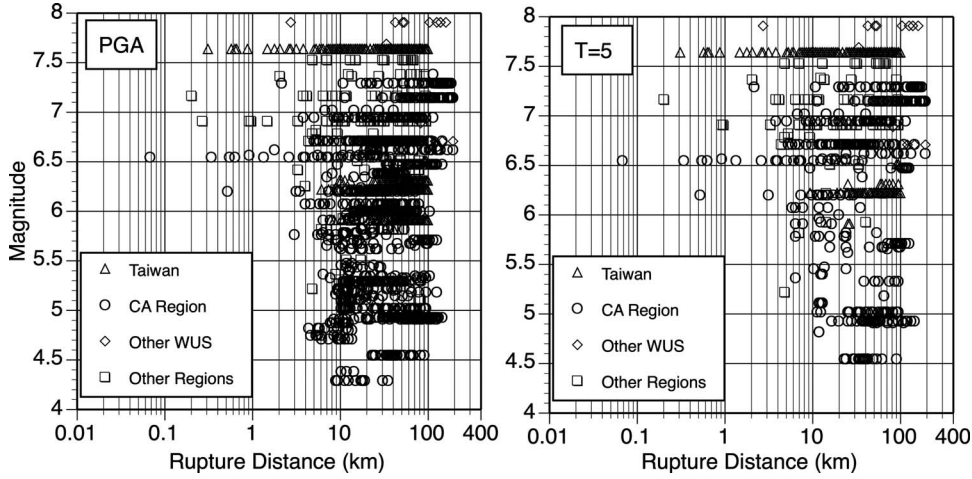
**Figure 2.** Distribution of magnitude-distance pairs for PGA and T=5 sec.

wall effect model is improved so that it will vary smoothly based on the source properties (M, dip, depth) and site location; and (5) the effects of nonlinear site response are incorporated into the standard deviation.

Incorporating these five changes has made the functional form of our ground-motion model much more complicated than in our previous model. In some cases, these changes lead to significant changes in the median and standard deviation of the ground-motion. For example, the buried rupture effect can change the median ground-motion by up to a factor of 2 for short periods; the soil depth effect can change the median ground-motion by up to a factor of 4 for long periods; the improved smoothing of the hanging-wall effect can change the median ground motion on the HW by up to a factor of 2 for short periods; and accounting for nonlinear effects in the standard deviation can reduce the standard deviation by up to 0.18 natural log units. The new ground-motion data and the analytical model results allow for robust estimation of these effects. We did not add the additional complexity to the model without good cause. We believe that these changes represent major improvements to our previous ground-motion model that justifies the additional complexity in our model.

## EQUATIONS FOR THE MEDIAN GROUND MOTION

The model for the median ground motion is given by:

$$\ln Sa(g) = f_1(M,R_{rup}) + a_{12}F_{RV} + a_{13}F_{NM} + a_{15}F_{AS} + f_5(P\hat{G}A_{1100}, V_{S30})$$
$$+ F_{HW}f_4(R_{jb}, R_{rup}, R_x, W, \delta, Z_{TOR}, M) + f_6(Z_{TOR}) + f_8(R_{rup}, M) + f_{10}(Z_{1.0}, V_{S30})$$

$$(1)$$

The parameters in Equation 1 are defined in Table 2.

**Table 2.** Definition of parameters used in the regression analysis

| Parameter | Definition | Notes |
|---|---|---|
| $M$ | Moment magnitude | |
| $R_{rup}$ | Rupture distance (km) | |
| $R_{jb}$ | Joyner-Boore distance (km) | |
| $R_x$ | Horizontal distance (km) from top edge of rupture | Measured perpendicular to the fault strike |
| $Z_{TOR}$ | Depth-to -top of rupture (km) | |
| $F_{RV}$ | Flag for reverse faulting earthquakes | 1 for reverse and reverse/oblique earthquakes defined by rake angles between 30 and 150 degrees, 0 otherwise |
| $F_{NM}$ | Flag for normal faulting earthquakes | 1 for normal earthquakes defined by rake angles between $-60$ and $-120$ degrees, 0 otherwise |
| $F_{AS}$ | Flag for aftershocks | 1 for aftershocks, 0 for mainshocks, foreshocks, and swarms (see Table 1) |
| $F_{HW}$ | Flag for hanging wall sites | 1 for sites on the hanging wall side of the fault, 0 otherwise. The boundary between the FW and HW is defined by the vertical projection of the top of the rupture. For dips of 90 degrees, $F_{HW}=0$ |
| $\delta$ | Fault dip in degrees | |
| $V_{S30}$ | Shear-wave velocity over the top 30 m (m/s) | |
| $Z_{1.0}$ | Depth to $V_S=1.0$ km/s at the site (m) | |
| $P\hat{G}A_{1100}$ | Median peak acceleration (g) for $V_{S30}=1100$ m/s | |
| $W$ | Down-dip rupture width (km) | |

The functional forms for $f_1, f_4, f_5, f_6, f_7, f_8$, and $f_{10}$ are given below.

**Base Model**

The base form of the magnitude and distance dependence for strike-slip earthquakes is the same as our 1997 model and is given by:

$$f_1(M,R_{rup}) = \begin{cases} a_1 + a_4(M-c_1) + a_8(8.5-M)^2 + [a_2+a_3(M-c_1)]\ln(R) & \text{for } M \leqslant c_1 \\ a_1 + a_5(M-c_1) + a_8(8.5-M)^2 + [a_2+a_3(M-c_1)]\ln(R) & \text{for } M > c_1 \end{cases}$$

$$(2)$$

where
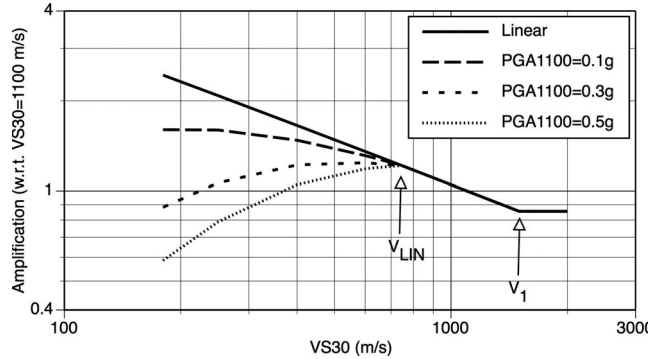
**Figure 3.** Example of the $V_{S3}0$ scaling for T=0.2 sec.

$$R = \sqrt{R_{rup}^2 + c_4^2}. \tag{3}$$

Four of the Chi-Chi (EQID 172, 173, 174, and 175) show a much more negative distance slope (e.g., steeper slope) than the other earthquakes in our data set. Given this difference, we did not want these data to have a large impact on the distance scaling of our model. Therefore, we included a separate coefficient for the ln(R) term for these four aftershocks (see Abrahamson and Silva 2008). We did not simply exclude the data for these four Chi-Chi aftershocks from our data set because they are important for constraining other aspects of the ground motion model such as site response and intra-event variability.

## Site Response Model

Our 1997 model included nonlinear soil response effects for generic soil sites. In our new model, the site is characterized by $V_{S30}$, so the nonlinear soil model was modified to incorporate a $V_{S30}$ dependence. We define a shear-wave velocity, $V_{LIN}$, above which the site response is linear. The model for the nonlinear site response was selected so that it becomes proportional to $\ln(V_{S30})$ as the input motion ($\hat{PGA}_{1100}$) becomes small and as the $V_{S30}$ approaches to $V_{LIN}$. We define a second shear-wave velocity, $V_1$, above which there is no scaling with $V_{S30}$. An example of the relation of the $V_{LIN}$ and $V_1$ parameters to the site response scaling is shown in Figure 3. For $V_{S30} > V_{LIN}$, there is no dependence on the $PGA_{1100}$; for $V_{S30} > V_1$, there is no dependence on $V_{S30}$.

We adopted the form of the nonlinear site response developed by Walling et al. (2008):

$$f_5(P\hat{G}A_{1100}, V^*_{S30}) = \begin{cases} a_{10} \ln\left(\dfrac{V^*_{S30}}{V_{LIN}}\right) - b \ln(P\hat{G}A_{1100} + c) \\[2ex] \quad + b \ln\left(P\hat{G}A_{1100} + c\left(\dfrac{V^*_{S30}}{V_{lin}}\right)^n\right) & \text{for } V_{S30} < V_{LIN} \\[2ex] (a_{10} + bn)\ln\left(\dfrac{V^*_{S30}}{V_{LIN}}\right) & \text{for } V_{S30} \geq V_{LIN} \end{cases} \quad (4)$$

where

$$V^*_{S30} = \begin{cases} V_{S30} & \text{for } V_{S30} < V_1 \\ V_1 & \text{for } V_{S30} \geq V_1 \end{cases} \quad (5)$$

and

$$V_1 = \begin{cases} 1500 \text{ m/s} & \text{for } T \leq 0.50 \text{ sec} \\ \exp[8.0 - 0.795 \ln(T/0.21)] & \text{for } 0.50 \text{ sec} < T \leq 1 \text{ sec} \\ \exp[6.76 - 0.297 \ln(T)] & \text{for } 1 \text{ sec} < T < 2 \text{ sec} \\ 700 \text{ m/s} & \text{for } T \geq 2 \text{ sec} \\ 862 \text{ m/s} & \text{for PGV} \end{cases} \quad (6)$$

The nonlinear site response terms $(b, c, n, V_{LIN})$ were constrained by the results of the 1-D analytical site response model using the Peninsula Range soil model (Walling et al. 2008). Only the $a_{10}$ term was estimated in the regression analysis.

**Hanging-Wall Model**

Our 1997 model included a hanging wall (HW) factor, but the model lead to jumps in the HW scaling for some cases and it was not clear how to apply the model for steeply dipping faults. To avoid these shortcomings, the new model includes five tapers to produce a smoothly varying HW effect. The model for the HW effect is given by:

$$f_4(R_{jb}, R_{rup}, \delta, Z_{TOR}, M, W) = a_{14} T_1(R_{jb}) T_2(R_x, W, \delta) T_3(R_x, Z_{TOR}) T_4(M) T_5(\delta) \quad (7)$$

where

$$T_1(R_{jb}) = \begin{cases} 1 - \dfrac{R_{jb}}{30} & \text{for } R_{jb} < 30 \text{ km} \\[2ex] 0 & \text{for } R_{jb} \geq 30 \text{ km} \end{cases} \quad (8)$$

$$T_2(R_x, W, \delta) = \begin{cases} 0.5 + \dfrac{R_x}{2W\cos(\delta)} & \text{for } R_x \leq W\cos(\delta) \\[2ex] 1 & \text{for } R_x > W\cos(\delta), \text{or } \delta = 90 \end{cases} \quad (9)$$

$$T_3(R_x, Z_{TOR}) = \begin{cases} 1 & \text{for } R_x \geq Z_{TOR} \\ \dfrac{R_x}{Z_{TOR}} & \text{for } R_x < Z_{TOR} \end{cases} \tag{10}$$

$$T_4(M) = \begin{cases} 0 & \text{for } M \leq 6 \\ M - 6 & \text{for } 6 < M < 7 \\ 1 & \text{for } M \geq 7 \end{cases} \tag{11}$$

$$T_5(\delta) = \begin{cases} 1 - \dfrac{\delta - 70}{20} & \text{for } \delta \geq 70 \\ 1 & \text{for } \delta < 70 \end{cases} \tag{12}$$

The first three tapers ($T_1$, $T_2$, and $T_3$) were constrained by the 1-D rock simulations and by the data from the Chi-Chi mainshock. The last two tapers ($T_4$ and $T_5$) were constrained by the events with well-recorded HW effects. Only the $a_{14}$ term was estimated in the regression analysis.

**Depth-to-Top of Rupture Model**

The Abrahamson and Silva (1997) model did not include a depth-to-top of rupture faulting dependence. Differences in the ground motions for surface and buried ruptures have been postulated by Somerville and Pitarka (2006). A key issue for incorporating a depth-to-top of rupture dependence is that there is a correlation of magnitude and depth-to-top of rupture: large earthquakes tend to rupture to the surface, whereas small earthquakes tend to be at depth. To address this correlation issue, we evaluated the depth dependence using a limited magnitude range (M5-M6) and found that there was still is a clear depth-to-top of rupture dependence (see Abrahamson and Silva 2008). Therefore, we included a depth-top-top of rupture dependence in our new model:

$$f_6(Z_{TOR}) = \begin{cases} \dfrac{a_{16} Z_{TOR}}{10} & \text{for } Z_{TOR} < 10 \text{ km} \\ \\ a_{16} & \text{for } Z_{TOR} \geq 10 \text{ km} \end{cases} \tag{13}$$

**Large Distance Model**

The NGA data set does not contain many recordings from small magnitude (M4-M5) earthquakes at large distances ($R_{rup} > 100$ km). As a result, the distance attenuation is not well constrained for moderate magnitudes. Our previous model did not address this data set deficiency. There is a large amount of data from moderate magnitude earthquakes recorded at large distances from networks that are not part of the traditional strong motion networks and were not included in the NGA data set. Broadband networks recordings from three small (M4) California earthquakes were used to constrain the large distance attenuation for small and moderate magnitude earthquakes (Abrahamson and Silva 2008). Based on these data, the large distance attenuation of the moderate magnitude earthquakes is modeled by

$$f_8(R_{rup}, M) = \begin{cases} 0 & \text{for } R_{rup} < 100 \text{ km} \\ a_{18}(R_{rup} - 100)T_6(M) & \text{for } R_{rup} \geq 100 \text{ km} \end{cases} \quad (14)$$

where

$$T_6(M) = \begin{cases} 1 & \text{for } M < 5.5 \\ 0.5(6.5 - M) + 0.5 & \text{for } 5.5 \leq M \leq 6.5 \\ 0.5 & \text{for } M > 6.5 \end{cases} \quad (15)$$

All of these terms are constrained outside of the regression analysis.

**Soil Depth Model**

Our previous model made no distinction between shallow soil sites and deep soil sites. A key difficulty has been that the soil depths have not been well determined for the strong motion data set. The NGA data set contains estimates of the depth of the soil (e.g., $Z_{1.0}$) for about $1/4$ of the data, but some significant inconsistencies between the $V_{S30}$ and soil depths indicate that this parameter is not well constrained.

The analytical models show a strong dependence of the long-period ground motion on the soil depth. We consider many of the $Z_{1.0}$ estimates in the flat-file to be unreliable, but we believe that there should be a soil-depth dependence for long periods. Therefore, the soil-depth scaling was completely constrained by the analytical site response models. The 1-D site response results (Silva 2005) were used to constrain the scaling with soil depth for shallow soil sites ($Z_{1.0} < 200$ m) and the 3-D basin response modeling results (Day et al. 2006) were used to constrain the scaling with soil depth for deep soil sites ($Z_{1.0} > 200$ m). The model for the scaling with soil depth is given by

$$f_{10}(Z_{1.0}, V_{S30}) = a_{21} \ln\left(\frac{Z_{1.0} + c_2}{\hat{Z}_{1.0}(V_{S30}) + c_2}\right) + \begin{cases} a_{22} \ln\left(\dfrac{Z_{1.0}}{200}\right) & \text{for } Z_{1.0} \geq 200 \\ 0 & \text{for } Z_{1.0} < 200 \end{cases} \quad (16)$$

where $\hat{Z}_{1.0}(V_{S30})$ is the median $Z_{1.0}$ (in m) given by

$$\ln(\hat{Z}_{1.0}(V_{S30})) = \begin{cases} 6.745 & \text{for } V_{S30} < 180 \text{ m/s} \\ 6.745 - 1.35 \ln\left(\dfrac{V_{S30}}{180}\right) & \text{for } 180 \leq V_{S30} \leq 500 \text{ m/s} \\ 5.394 - 4.48 \ln\left(\dfrac{V_{S30}}{500}\right) & \text{for } V_{S30} > 500 \text{ m/s} \end{cases} \quad (17)$$

$$a_{21} = \begin{cases} 0 & \text{for } V_{S30} \geq 1000 \\[2em] \dfrac{-(a_{10}+bn)\ln\left(\dfrac{V^*_{S30}}{\min(V_1,1000)}\right)}{\ln\left(\dfrac{Z_{1.0}+c_2}{\hat{Z}_{1.0}+c_2}\right)} & \text{for } (a_{10}+bn)\ln\left(\dfrac{V^*_{S30}}{\min(V_1,1000)}\right) \\[2em] & \quad + e_2 \ln\left(\dfrac{Z_{1.0}+c_2}{\hat{Z}_{1.0}+c_2}\right) < 0 \\[1em] e_2 & \text{otherwise} \end{cases}$$

(18)

$$e_2 = \begin{cases} 0 & \text{for } T < 0.35 \text{ sec } \textit{or } V_{S30} > 1000 \\[1em] -0.25\ln\left(\dfrac{V_{S30}}{1000}\right)\ln\left(\dfrac{T}{0.35}\right) & \text{for } 0.35 \leq T \leq 2 \text{ sec} \\[1em] -0.25\ln\left(\dfrac{V_{S30}}{1000}\right)\ln\left(\dfrac{2}{0.35}\right) & \text{for } T > 2 \text{ sec} \end{cases}$$

(19)

and

$$a_{22} = \begin{cases} 0 & \text{for } T < 2 \text{ sec} \\ 0.0625(T-2) & \text{for } T \geq 2 \text{ sec} \end{cases}$$

(20)

For PGV, the $a_{21}$ and $a_{22}$ values are computed using T=1 sec in Equation 18 and Equation 20. A constraint on the model is that the ground motion for shallow soil sites does not fall below the ground motion for $V_{S30}$=1000 m/s.

## Constant Displacement Model

At long spectral periods, the response spectrum for rock sites will reach a constant displacement. The period at which the rock ($V_{S30}$=1100 m/s) spectrum reaches a constant displacement is denoted $T_D$. The point-source stochastic model and the 1-D rock simulations were used to evaluate the magnitude-dependence of $T_D$. The resulting model for $T_D$ is given by:

$$\log_{10}(T_D) = -1.25 + 0.3M$$

(21)

For spectral periods greater than $T_D$, the rock spectral acceleration is first computed at T=$T_D$. The rock spectral acceleration at period T is then computed by scaling the rock spectral acceleration at period $T_D$ by $(T_D/T)^2$ for constant spectral displacement. The site response and soil depth scaling is then applied to the rock spectral acceleration. The computation of the spectral acceleration for $T > T_D$ is shown in Equation 22.

$$Sa(T) = \begin{cases} Sa(T) \text{ from Eq. (1)} & \text{for } T \leq T_D \\ Sa(T_D, V_{S30} = 1100) \dfrac{T_D^2}{T^2} + f_5(P\hat{G}A_{1100}, V_{S30}, T) + f_{10}(Z_{1.0}, V_{S30}, T) & \text{for } T > T_D \end{cases}$$

(22)

## EQUATIONS FOR STANDARD DEVIATION

The random-effects model was used for the regression analysis following the procedure described by Abrahamson and Youngs (1992) with modifications for the effects of the nonlinear site response on the standard deviations as described in Abrahamson and Silva (2008). The random-effects method leads to two types of residuals: inter-event residuals and intra-event residuals. The inter-event residuals are for outcrop rock motion.

The standard deviation in the linear site response range is dependent on the earthquake magnitude. In the nonlinear range, if the input rock motion is higher than average, then the amplification will be smaller and if the input rock motion is lower than average, then the amplification will be greater. As a result, the both the intra-event and inter-event variability of the soil ground motion is reduced for large $P\hat{G}A_{1100}$. Incorporating the effect of the soil nonlinearity on the inter-event and intra-event standard deviations leads to complicated forms that depends on the $P\hat{G}A_{1100}$ and on the correlation of the residuals at PGA and other spectral periods. The amplitude dependence of the intra-event and inter-event standard deviations is computed through simple propagation of variance. To propagate the variance, additional intermediate standard deviations are defined: $\sigma_0$ and $\tau_0$ are the intra-event and inter-event standard deviation of the observed ground motions for low levels of outcrop rock motion (e.g., linear site response range) which come directly from the regression analysis; $\sigma_B$ and $\tau_B$ are the intra-event and inter-event standard deviations of the input rock motion; and $\sigma_{amp}$ as the intra-event variability of the site amplification factors. The observed intra-event variability for the linear range is a combination of the intra-event variability of the input rock motion and the variability of the site amplification. Assuming these terms are independent:

$$\sigma_B(M,T) = \sqrt{\sigma_0^2(M,T) - \sigma_{Amp}^2(T)}$$

(23)

We assume that $\sigma_{amp}(T) = 0.3$ for all periods based on the 1-D site response simulation results. For the inter-event variability, the observed inter-event variability for the linear range is just the inter-event variability of the input rock motion, so $\tau_B(M,T) = \tau_0(M,T)$.

Propagating the variances, the intra-event standard deviation is given by

$$\sigma(T,M,P\hat{G}A_{1100},V_{S30}) = \begin{bmatrix} \sigma_0^2(M,T) + \sigma_{\mathrm{Amp}}^2(T) \\[6pt] + \left( \dfrac{\partial \ln \mathrm{Amp}(T,P\hat{G}A_{1100},V_{S30})}{\partial \ln PGA_{1100}} \right)^2 \sigma_B^2(M,PGA) \\[6pt] + 2 \left( \dfrac{\partial \ln \mathrm{Amp}(T,P\hat{G}A_{1100},V_{S30})}{\partial \ln PGA_{1100}} \right) \\[6pt] \times \sigma_B(M,T)\sigma_B(M,PGA)\rho_{\varepsilon/\sigma}(T,PGA) \end{bmatrix}^{1/2}$$

$$(24)$$

and the inter-event standard deviation is given by

$$\tau(T,M,P\hat{G}A_{1100},V_{S30}) = \begin{bmatrix} \tau_0^2(M,T) + \left( \dfrac{\partial \ln \mathrm{Amp}(T,P\hat{G}A_{1100},V_{S30})}{\partial \ln PGA_{1100}} \right)^2 \tau_B^2(M,PGA) \\[6pt] + 2 \left( \dfrac{\partial \ln \mathrm{Amp}(T,P\hat{G}A_{1100},V_{S30})}{\partial \ln PGA_{1100}} \right) \\[6pt] \times \tau_B(M,T)\tau_B(M,PGA)\rho_{\eta/\tau}(T,PGA) \end{bmatrix}^{1/2}$$

$$(25)$$

where

$$\frac{\partial \ln \mathrm{Amp}(T,P\hat{G}A_{1100},V_{S30})}{\partial \ln PGA_{1100}}$$

$$= \begin{cases} 0 & \textit{for } V_{S30} \geqslant V_{LIN} \\[10pt] \dfrac{-b(T)P\hat{G}A_{1100}}{P\hat{G}A_{1100}+c} + \dfrac{1}{P\hat{G}A_{1100}+c\left(\dfrac{V_{S30}}{V_{LIN}}\right)^n} & \textit{for } V_{S30} < V_{LIN} \end{cases}$$

$$(26)$$

$$\sigma_0(M) = \begin{cases} s_1 & \textit{for } M < 5 \\[6pt] s_1 + \left( \dfrac{s_2 - s_1}{2} \right)(M-5) & \textit{for } 5 \leqslant M \leqslant 7 \\[6pt] s_2 & \textit{for } M > 7 \end{cases}$$

$$(27)$$

and

$$\tau_0(M) = \begin{cases} s_3 & \textit{for } M < 5 \\[6pt] s_3 + \left( \dfrac{s_4 - s_3}{2} \right)(M-5) & \textit{for } 5 \leqslant M \leqslant 7 \\[6pt] s_4 & \textit{for } M > 7 \end{cases}$$

$$(28)$$

**Table 3.** Constraints on the model parameters

| Parameter | Description | Estimation |
|---|---|---|
| $a_1$ | Constant | Regression |
| $a_2$ | Distance slope | Regression |
| $a_3$ | Magnitude dependent distance slope | PGA regression |
| $a_4$ | Linear magnitude scaling, $M < c_1$ | PGA regression |
| $a_5$ | Linear magnitude scaling, $M >= c_1$ | Constrained to full saturation for PGA |
| $a_8$ | Quadratic magnitude scaling | Regression |
| $a_{10}$ | Linear site response scaling | Regression |
| $a_{12}$ | RV style-of-faulting factor | Regression |
| $a_{13}$ | NML style-of-faulting factor | Regression (new) |
| $a_{14}$ | HW factor | Regression |
| $a_{15}$ | Aftershock factor | Regression (new) |
| $a_{16}$ | Depth-to-top scaling | Regression (new) |
| $a_{18}$ | Large distance scaling for small M | Constrained by 3 small M eqk |
| $a_{21}$ | Shallow soil depth scaling factor | Constrained by 1-D site response |
| $a_{22}$ | Deep soil depth scaling factor | Constrained by 3-D basin simulation |
| $c_1$ | Break in magnitude scaling | Constrained by hard-rock simulations and empirical data |
| $c_4$ | Fictitious depth | PGA regression |
| N | Non-linear soil response term | Constrained by 1-D site simulation |
| c | Non-linear soil response term | Constrained by 1-D site simulation |
| b | Slope of nonlinear soil response | Constrained by 1-D site simulation |
| $V_{LIN}$ | Linear scaling for $V_{S30} > V_{LIN}$ | Constrained by 1-D site simulation |
| $c_2$ | Shallow soil depth scaling term | Constrained by 1-D site simulation |

## REGRESSION RESULTS

Our model includes a large number of coefficients; a recurring issue raised regarding our model is the model complexity. There has been a concern that the model is over-parameterized such that the parameters cannot be reliably estimated from the empirical data, particularly at long periods ($T > 5$ sec) for which the data set becomes much smaller (Figure 1). Much of the model complexity is associated with nonlinear site response and soil depth scaling which are fully constrained outside of the regression analysis. Table 3 indicates which parameters are constrained and which are estimated as part of the regression. For periods greater than 5 seconds, several parameters ($a_2$, $a_{12}$, $a_{13}$, $a_{16}$, and $a_{18}$) are fixed at their values for 2–4 seconds since they could not be constrained by the data. Compared with our 1997 model, our new model includes only three additional coefficients that are computed in the regression: style-of-faulting factor for normal faults ($a_{13}$), aftershock factor ($a_{15}$), and depth-to-top of rupture scaling ($a_{16}$).

To arrive at a smooth model, the coefficients were smoothed in a series of steps. The details of this smoothing are described in Abrahamson and Silva (2008). The final smoothed coefficients for the median ground motion are listed in Tables 4, 5a, and 5b. The coefficients for the standard deviation models are listed in Table 6. The standard

**Table 4.** Period-independent constants for the median ground motion

| $c_1$ | $c_4$ | $a_3$ | $a_4$ | $a_5$ | $N$ | $c$ | $c_2$ |
|-------|-------|-------|--------|--------|------|------|------|
| 6.75 | 4.5 | 0.265 | −0.231 | −0.398 | 1.18 | 1.88 | 50 |

deviation terms were reduced to account for the contribution of uncertainty in the independent parameters ($M$, $R_{rup}$, $Z_{TOR}$, $V_{S30}$) to the computed standard deviation (Abrahamson and Silva 2008). The uncertainty in $V_{S30}$ had the largest impact on the standard deviations. The uncertainty in $M$, $R_{rup}$, $Z_{TOR}$ had only a minor impact on the standard deviation.

The standard errors of the estimated parameters and the correlations of the estimates are given in Abrahamson and Silva (2008). Correlations of the inter-event and intra-event residuals, required for vector hazard and conditional mean spectra, are also given in Abrahamson and Silva (2008).

**Table 5a.** Coefficients for the median ground motion

| Parameter | $V_{LIN}$ | $b$ | $a_1$ | $a_2$ | $a_8$ | $a_{10}$ | $a_{12}$ | $a_{13}$ |
|-----------|-----------|-----|-------|-------|-------|----------|----------|----------|
| PGA | 865.1 | −1.186 | 0.804 | −0.9679 | −0.0372 | 0.9445 | 0.0000 | −0.0600 |
| Sa(T=0.010) | 865.1 | −1.186 | 0.811 | −0.9679 | −0.0372 | 0.9445 | 0.0000 | −0.0600 |
| Sa(T=0.020) | 865.1 | −1.219 | 0.855 | −0.9774 | −0.0372 | 0.9834 | 0.0000 | −0.0600 |
| Sa(T=0.030) | 907.8 | −1.273 | 0.962 | −1.0024 | −0.0372 | 1.0471 | 0.0000 | −0.0600 |
| Sa(T=0.040) | 994.5 | −1.308 | 1.037 | −1.0289 | −0.0315 | 1.0884 | 0.0000 | −0.0600 |
| Sa(T=0.050) | 1053.5 | −1.346 | 1.133 | −1.0508 | −0.0271 | 1.1333 | 0.0000 | −0.0600 |
| Sa(T=0.075) | 1085.7 | −1.471 | 1.375 | −1.0810 | −0.0191 | 1.2808 | 0.0000 | −0.0600 |
| Sa(T=0.10) | 1032.5 | −1.624 | 1.563 | −1.0833 | −0.0166 | 1.4613 | 0.0000 | −0.0600 |
| Sa(T=0.15) | 877.6 | −1.931 | 1.716 | −1.0357 | −0.0254 | 1.8071 | 0.0181 | −0.0600 |
| Sa(T=0.20) | 748.2 | −2.188 | 1.687 | −0.9700 | −0.0396 | 2.0773 | 0.0309 | −0.0600 |
| Sa(T=0.25) | 654.3 | −2.381 | 1.646 | −0.9202 | −0.0539 | 2.2794 | 0.0409 | −0.0600 |
| Sa(T=0.30) | 587.1 | −2.518 | 1.601 | −0.8974 | −0.0656 | 2.4201 | 0.0491 | −0.0600 |
| Sa(T=0.40) | 503.0 | −2.657 | 1.511 | −0.8677 | −0.0807 | 2.5510 | 0.0619 | −0.0600 |
| Sa(T=0.50) | 456.6 | −2.669 | 1.397 | −0.8475 | −0.0924 | 2.5395 | 0.0719 | −0.0600 |
| Sa(T=0.75) | 410.5 | −2.401 | 1.137 | −0.8206 | −0.1137 | 2.1493 | 0.0800 | −0.0600 |
| Sa(T=1.0) | 400.0 | −1.955 | 0.915 | −0.8088 | −0.1289 | 1.5705 | 0.0800 | −0.0600 |
| Sa(T=1.5) | 400.0 | −1.025 | 0.510 | −0.7995 | −0.1534 | 0.3991 | 0.0800 | −0.0600 |
| Sa(T=2.0) | 400.0 | −0.299 | 0.192 | −0.7960 | −0.1708 | −0.6072 | 0.0800 | −0.0600 |
| Sa(T=3.0) | 400.0 | 0.000 | −0.280 | −0.7960 | −0.1954 | −0.9600 | 0.0800 | −0.0600 |
| Sa(T=4.0) | 400.0 | 0.000 | −0.639 | −0.7960 | −0.2128 | −0.9600 | 0.0800 | −0.0600 |
| Sa(T=5.0) | 400.0 | 0.000 | −0.936 | −0.7960 | −0.2263 | −0.9208 | 0.0800 | −0.0600 |
| Sa(T=7.5) | 400.0 | 0.000 | −1.527 | −0.7960 | −0.2509 | −0.7700 | 0.0800 | −0.0600 |
| Sa(T=10.0) | 400.0 | 0.000 | −1.993 | −0.7960 | −0.2683 | −0.6630 | 0.0800 | −0.0600 |
| PGV | 400.0 | −1.955 | 5.7578 | −0.9046 | −0.1200 | 1.5390 | 0.0800 | −0.0600 |

**Table 5b.** Coefficients for the median ground motion

| Parameter | $a_{14}$ | $a_{15}$ | $a_{16}$ | $a_{18}$ |
|---|---|---|---|---|
| PGA | 1.0800 | −0.3500 | 0.9000 | −0.0067 |
| Sa(T=0.010) | 1.0800 | −0.3500 | 0.9000 | −0.0067 |
| Sa(T=0.020) | 1.0800 | −0.3500 | 0.9000 | −0.0067 |
| Sa(T=0.030) | 1.1331 | −0.3500 | 0.9000 | −0.0067 |
| Sa(T=0.040) | 1.1708 | −0.3500 | 0.9000 | −0.0067 |
| Sa(T=0.050) | 1.2000 | −0.3500 | 0.9000 | −0.0076 |
| Sa(T=0.075) | 1.2000 | −0.3500 | 0.9000 | −0.0093 |
| Sa(T=0.10) | 1.2000 | −0.3500 | 0.9000 | −0.0093 |
| Sa(T=0.15) | 1.1683 | −0.3500 | 0.9000 | −0.0093 |
| Sa(T=0.20) | 1.1274 | −0.3500 | 0.9000 | −0.0083 |
| Sa(T=0.25) | 1.0956 | −0.3500 | 0.9000 | −0.0069 |
| Sa(T=0.30) | 1.0697 | −0.3500 | 0.9000 | −0.0057 |
| Sa(T=0.40) | 1.0288 | −0.3500 | 0.8423 | −0.0039 |
| Sa(T=0.50) | 0.9971 | −0.3191 | 0.7458 | −0.0025 |
| Sa(T=0.75) | 0.9395 | −0.2629 | 0.5704 | 0.0000 |
| Sa(T=1.0) | 0.8985 | −0.2230 | 0.4460 | 0.0000 |
| Sa(T=1.5) | 0.8409 | −0.1668 | 0.2707 | 0.0000 |
| Sa(T=2.0) | 0.8000 | −0.1270 | 0.1463 | 0.0000 |
| Sa(T=3.0) | 0.4793 | −0.0708 | −0.0291 | 0.0000 |
| Sa(T=4.0) | 0.2518 | −0.0309 | −0.1535 | 0.0000 |
| Sa(T=5.0) | 0.0754 | 0.0000 | −0.2500 | 0.0000 |
| Sa(T=7.5) | 0.0000 | 0.0000 | −0.2500 | 0.0000 |
| Sa(T=10.0) | 0.0000 | 0.0000 | −0.2500 | 0.0000 |
| PGV | 0.7000 | −0.3900 | 0.6300 | 0.0000 |

## RESIDUALS

The regression analysis described in Abrahamson and Silva (2008) included two additional terms to account for differences in the distance attenuation from four Chi-Chi aftershocks and from attenuation off the end of the rupture from the Chi-Chi mainshock. Those terms are not part of our final model for estimating ground motions in California so they are not included in Equation 1, but they are included in the computation of the residuals. A complete discussion of these additional terms is given in Abrahamson and Silva (2008).

A key issue for the NGA models has been the impact of data from outside of California, in particular the large amount of data from the Chi-Chi earthquake sequence. Use of the random-effects method accounts for the correlation in the data from a single earthquake and prevents well-recorded earthquakes from dominating the regression. Examples of the magnitude and depth-to-top dependence of the inter-event residuals for T=0.2 sec are shown in Figure 4. The residuals are separated by region and show that there is not a systematic trend in the residuals for the different regions. For M>7.5, the

**Table 6.** Coefficients for the standard deviation

| Parameter | $V_{S30}$ Estimated | | $V_{S30}$ Measured | | | | $\rho(T,PGA)$[a] |
|---|---|---|---|---|---|---|---|
| | $s_1$ | $s_2$ | $s_1$ | $s_2$ | $s_3$ | $s_4$ | |
| PGA | 0.590 | 0.470 | 0.576 | 0.453 | 0.470 | 0.300 | 1.000 |
| Sa(T=0.010) | 0.590 | 0.470 | 0.576 | 0.453 | 0.420 | 0.300 | 1.000 |
| Sa(T=0.02) | 0.590 | 0.470 | 0.576 | 0.453 | 0.420 | 0.300 | 1.000 |
| Sa(T=0.03) | 0.605 | 0.478 | 0.591 | 0.461 | 0.462 | 0.305 | 0.991 |
| Sa(T=0.04) | 0.615 | 0.483 | 0.602 | 0.466 | 0.492 | 0.309 | 0.982 |
| Sa(T=0.05) | 0.623 | 0.488 | 0.610 | 0.471 | 0.515 | 0.312 | 0.973 |
| Sa(T=0.075) | 0.630 | 0.495 | 0.617 | 0.479 | 0.550 | 0.317 | 0.952 |
| Sa(T=0.10) | 0.630 | 0.501 | 0.617 | 0.485 | 0.550 | 0.321 | 0.929 |
| Sa(T=0.15) | 0.630 | 0.509 | 0.616 | 0.491 | 0.550 | 0.326 | 0.896 |
| Sa(T=0.20) | 0.630 | 0.514 | 0.614 | 0.495 | 0.520 | 0.329 | 0.874 |
| Sa(T=0.25) | 0.630 | 0.518 | 0.612 | 0.497 | 0.497 | 0.332 | 0.856 |
| Sa(T=0.30) | 0.630 | 0.522 | 0.611 | 0.499 | 0.479 | 0.335 | 0.841 |
| Sa(T=0.40) | 0.630 | 0.527 | 0.608 | 0.501 | 0.449 | 0.338 | 0.818 |
| Sa(T=0.50) | 0.630 | 0.532 | 0.606 | 0.504 | 0.426 | 0.341 | 0.783 |
| Sa(T=0.75) | 0.630 | 0.539 | 0.602 | 0.506 | 0.385 | 0.346 | 0.680 |
| Sa(T=1.0) | 0.630 | 0.545 | 0.594 | 0.503 | 0.350 | 0.350 | 0.607 |
| Sa(T=1.5) | 0.615 | 0.552 | 0.566 | 0.497 | 0.350 | 0.350 | 0.504 |
| Sa(T=2.0) | 0.604 | 0.558 | 0.544 | 0.491 | 0.350 | 0.350 | 0.431 |
| Sa(T=3.0) | 0.589 | 0.565 | 0.527 | 0.500 | 0.350 | 0.350 | 0.328 |
| Sa(T=4.0) | 0.578 | 0.570 | 0.515 | 0.505 | 0.350 | 0.350 | 0.255 |
| Sa(T=5.0) | 0.570 | 0.587 | 0.510 | 0.529 | 0.350 | 0.350 | 0.200 |
| Sa(T=7.5) | 0.611 | 0.618 | 0.572 | 0.579 | 0.350 | 0.350 | 0.200 |
| Sa(T=10.0) | 0.640 | 0.640 | 0.612 | 0.612 | 0.350 | 0.350 | 0.200 |
| PGV | 0.590 | 0.470 | 0.576 | 0.453 | 0.420 | 0.300 | 0.740 |

[a] This applies to both $\rho_{\varepsilon/\sigma}(PGA,T)$ and $\rho_{\eta/\tau}(PGA,T)$

inter-event residuals are biased to negative values. This is a consequence of the constraint of full saturation. If allowed to fit the data, the model would have lead to oversaturation.

Examples of the distance, $V_{S30}$, and $PGA_{1100}$ dependence of the intra-event residuals for T=0.2 sec are shown in Figure 5. These figures show that there is no significant trend in the residuals. A complete set of residual plots for a wide range of spectral periods is given in Abrahamson and Silva (2008).
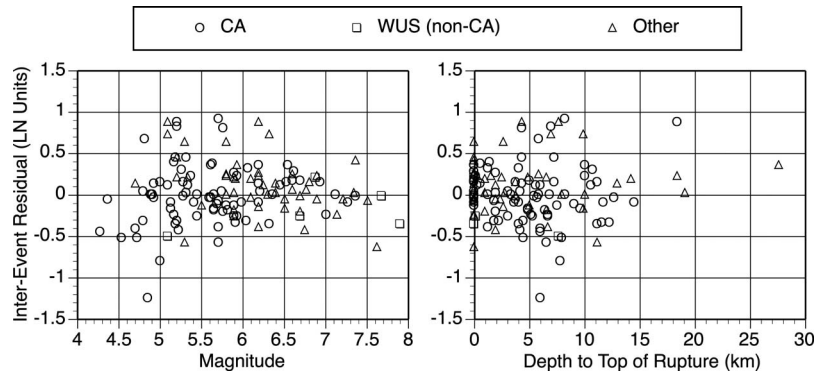
**Figure 4.** Interevent residuals for T=0.2 sec.

## MODEL RESULTS

### MEDIAN GROUND MOTION

The median response spectra for the current model are shown in Figure 6 for vertical strike-slip earthquakes at an $R_{JB}$ distance of 30 km. For this case, the $Z_{top}$ values are 6, 3, 1, and 0 for magnitudes 5, 6, 7, and 8, respectively. The $Z_{1.0}$ values are set at the median for the given $V_{S30}$ ($Z_{1.0}$=34 m, 144 m, and 492 m for $V_{S30}$=760, 550, and 270 m/s, respectively). Figure 6 shows that the median spectra from the current model
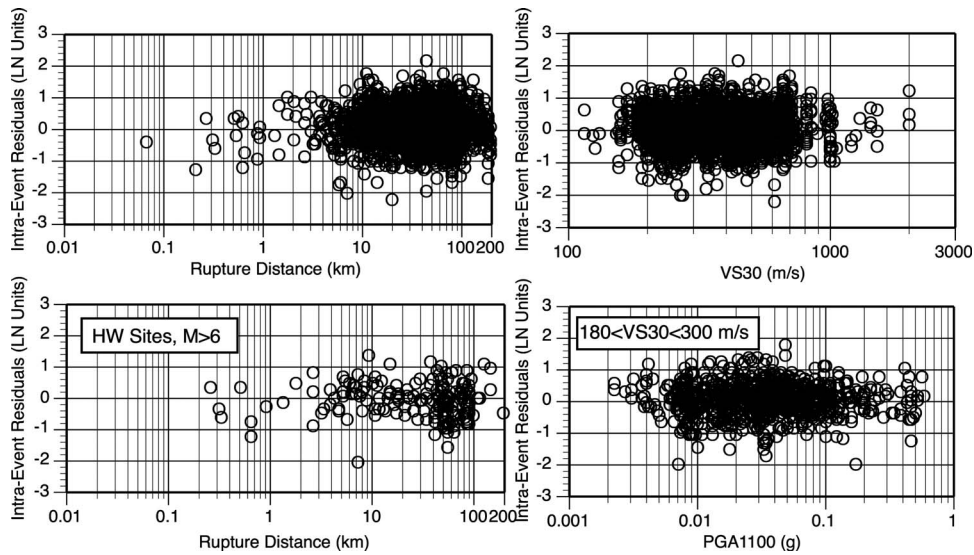


**Figure 5.** Intra-event residuals for T=0.2 sec.
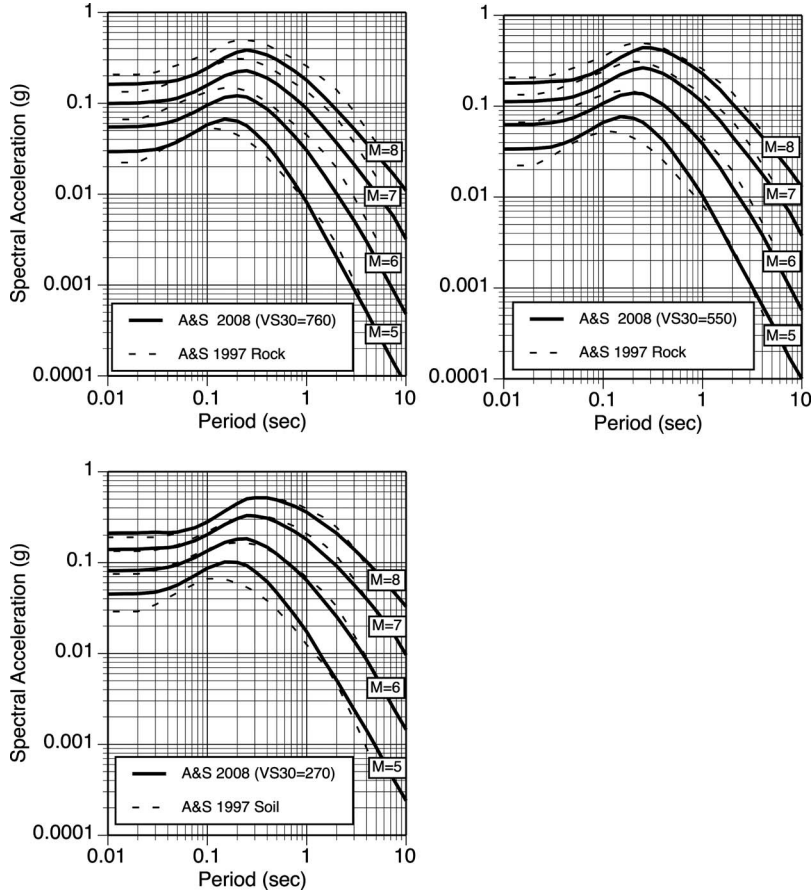
**Figure 6.** Comparison of the median spectral acceleration from the current model with the median from the Abrahamson and Silva (1997) model for vertical strike-slip earthquakes for $R_{JB}=30$ km.

are very similar to the spectra from our previous model (Abrahamson and Silva 1997) for soil sites ($V_{S30}=270$ m/s) at a distance of 30 km. Most of the data used by Abrahamson and Silva (1997) are from soil sites and the center of the data is near 30 km, so this agreement is expected.

Figure 6 also shows the comparison for the same case (strike-slip, 30 km), but for rock sites. The spectra for the current model are computed using $V_{S30}=760$ m/s for rock, consistent with national hazard maps. For rock sites, the ground motions from the current model are significantly lower than the previous model. Part of this difference is due to the definition of rock. For the current model, we have used $V_{S30}=760$ m/s for rock, whereas the generic rock used in Abrahamson and Silva (1997) corresponds to an average of about 550 m/s. The lower frame in Figure 6 compares the Abrahamson and Silva (1997) rock spectra to the current model using $V_{S30}=550$ m/s. With this lower
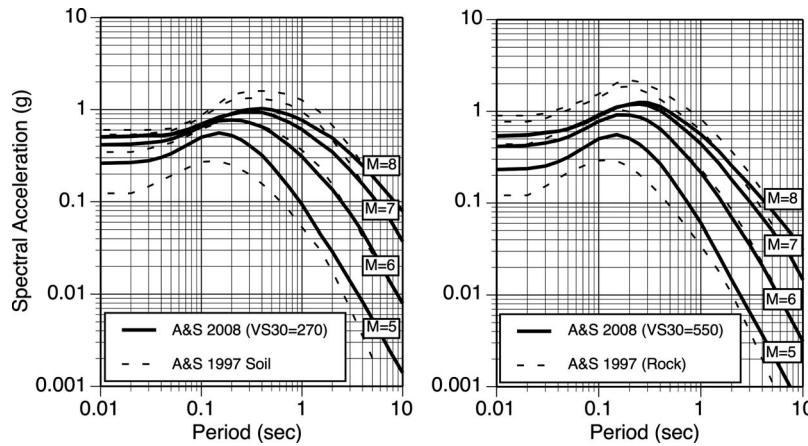
**Figure 7.** Comparison of the median spectral acceleration from the current model with the median from the Abrahamson and Silva (1997) model for vertical strike-slip earthquakes for $R_{JB}=1$ km.

velocity, the models are in close agreement for M6, but the current model still leads to smaller ground motions for M7 and M8. The ground motions for M5 are larger in the current model due to the scaling with $Z_{top}$.

The soil spectra for vertical strike-slip earthquakes for $R_{JB}=1$ km are shown in the left frame of Figure 7. For M6, the models are similar, but for larger magnitudes, the current model leads to lower median ground motion at this short distance, reflecting the lower ground motions observed at short distances in recent large-magnitude earthquakes. The rock spectra for this same case are shown in the right frame of Figure 7 using $V_{S30}=550$ m/s. The M6 spectrum for the current model is very similar to the previous model. At larger magnitudes, the saturation is stronger in the current model.

The distance scaling is shown in Figure 8 for PGA and spectral periods of 0.2, 1.0, and 3.0 seconds. In this figure, the median ground motion from vertical strike-slip earthquakes on rock site conditions ($V_{S30}=760$ m/s) is shown.

The magnitude scaling of the current model is shown in Figure 9 for vertical strike-slip earthquakes on rock site conditions ($V_{S30}=760$ m/s) for T=0.2 and T=3.0 seconds. The weak scaling of the short-period motion at short distances reflects the saturation with magnitude.

An example of the hanging-wall scaling is shown in Figure 10 for PGA on rock site conditions ($V_{S30}=760$ m/s) for an M6.7 reverse earthquake with a 45 degree dip. This figure shows that for surface ruptures, there is a step in the ground motion from the FW to the HW, but that for buried ruptures, there is a smooth transition. The short-period ground motion for buried ruptures is larger than the short period ground motion for surface ruptures at most locations even though the rupture distances are larger for the buried rupture. This is due to the scaling with $Z_{TOR}$.
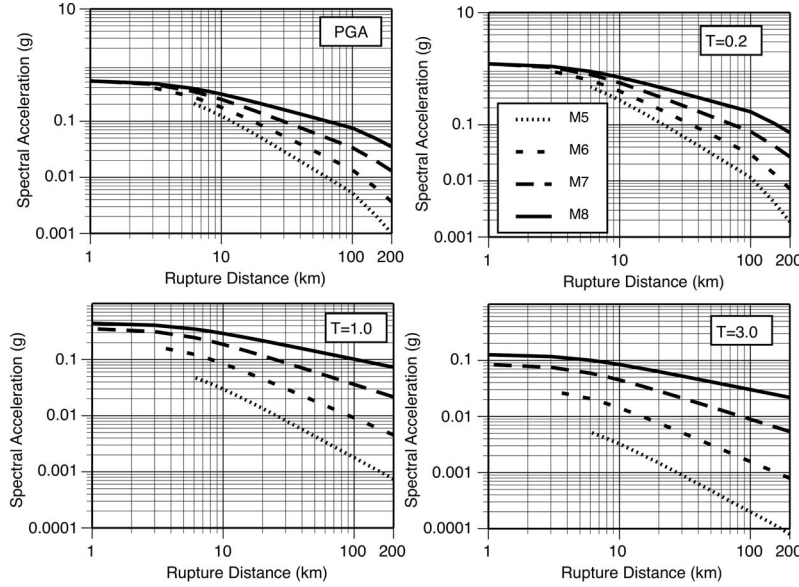
**Figure 8.** Comparison of the scaling with distance for the current model with the A&S (1997) model for strike-slip earthquakes and rock site conditions ($V_{S30}$=760 m/s).

Figure 11 shows the differences between FW and HW motions as a function of the rupture distance. It also shows the increase in the short-period ground-motion for buried ruptures as compared to surface ruptures. For the buried rupture example, the PGA increases as the site moves over the rupture even though the rupture distance is increasing.

The site response scaling for M7 vertical strike-slip earthquakes at a rupture distance of 30 km is shown in Figures 12 and 13: Figure 12 shows the dependence of the spectra on the $V_{S30}$ and Figure 13 shows that dependence of the spectra on the $Z_{1.0}$ for a soil site
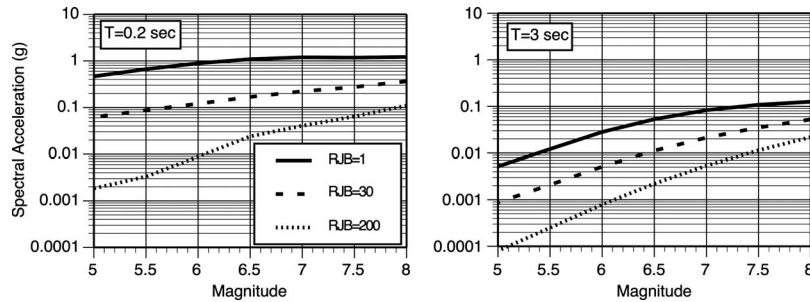


**Figure 9.** Magnitude scaling for strike-slip earthquakes and rock site condition ($V_{S30}$ =760 m/s) for T=0.2 sec and T=3 sec.
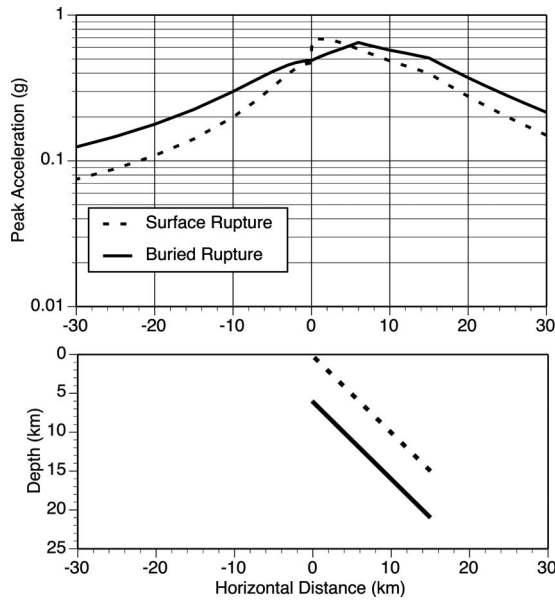
**Figure 10.** Attenuation of peak acceleration on the HW and FW for M6.7, rock ($V_{S30}$ =760 m/s) for buried and surface ruptures. The bottom panel shows a cross section of the rupture planes.
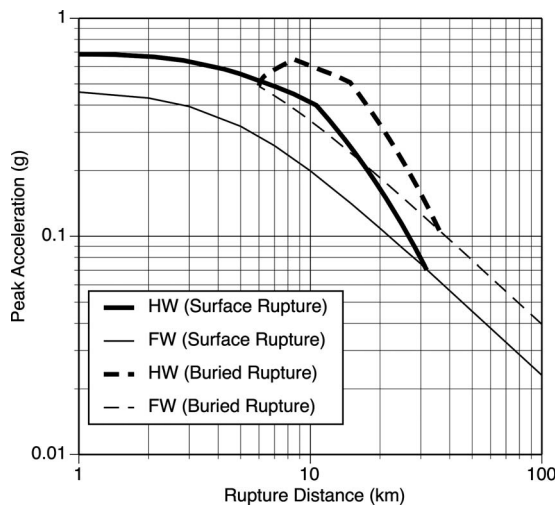


**Figure 11.** HW and FW effects on peak acceleration for M6.7, rock ($V_{S30}$=760 m/s) for the source geometry shown in Figure 10.
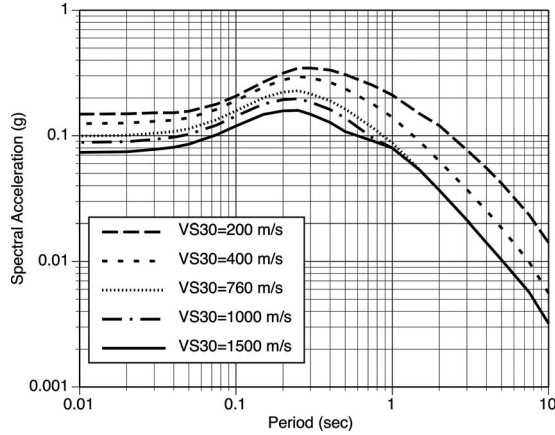
**Figure 12.** Example scaling with $V_{S30}$.

with $V_{S30}=270$ m/s. At long periods, there is a strong effect of the soil depth with about a factor of four difference in the ground motion between deep soil sites and shallow soil sites.

The Southern California Earthquake Center (SCEC) group on 3-D basin response developed amplification factors based on $Z_{1.0}$ only (Day et al. 2006). As shown in Figure 14, $V_{S30}$ is correlated with $Z_{1.0}$. Therefore, the $Z_{1.0}$ scaling from the SCEC model includes the combined effect of $V_{S30}$ scaling and $Z_{1.0}$ scaling. To compare our model with the SCEC amplification, we need to account for this correlation. For each $V_{S30}$ value, a range of $Z_{1.0}$ values is sampled assuming that $\ln(Z_{1.0})$ has a standard deviation of 0.7 ln units about the median curves shown in Figure 14. This gave a suite of $V_{S30}$, $Z_{1.0}$ pairs.
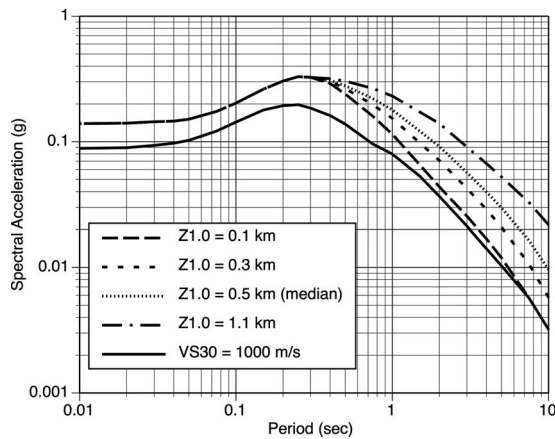


**Figure 13.** Example scaling with soil depth.
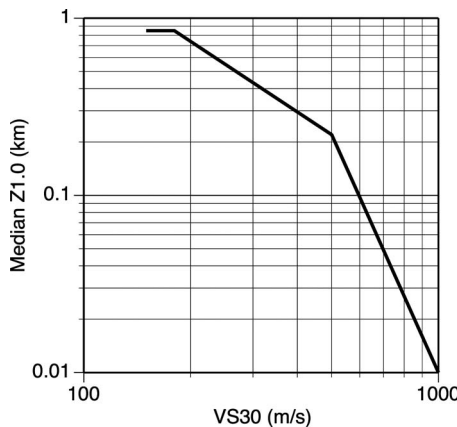
**Figure 14.** Relation between median $Z_{1.0}$ and $V_{S30}$.

For each pair, the amplification with respect to $V_{S30}=1100$ m/s and $Z_{1.0}=0$ m was computed using our NGA model. The amplifications were then fit to a function of $Z_{1.0}$ to estimate the total scaling with $Z_{1.0}$ from our model. The resulting net $Z_{1.0}$ scaling from our model is compared to the SCEC scaling in Figure 15 for periods of 3 and 10 seconds. For deep sites ($Z_{1.0}>200$ m), the $Z_{1.0}$ scaling in our model was constrained by the scaling from the SCEC model, shown by the agreement in the $Z_{1.0}$ scaling between our model and the SCEC model.

**STANDARD DEVIATION**

The period and magnitude dependence of the total standard deviation (combined inter-event and intra-event standard deviations) is shown in Figure 16 for vertical strike-slip earthquakes at a $R_{JB}$ distance of 30 km. For M5 at short periods, the standard deviations from the current model are similar to the standard deviation from Abrahamson and Silva (1997), but a long periods, the new model leads to smaller standard deviations as the magnitude dependence of the standard deviation decreases at long periods. For M7 at soil sites, the standard deviations at short periods ($T<2$ sec) are larger in the current model as compared to our previous model, reflecting the larger intra-event standard deviations observed in the recent large magnitude earthquakes. For rock sites, the short period standard deviations are larger than for soil sites. The reduction in the standard deviation for soil sites is due to the soil nonlinearity.

The effect of the soil nonlinearity on the standard deviation leads to a distance dependence of the standard deviation with smaller standard deviations at short distances. The distance dependence of the $T=0.2$ sec standard deviation is shown in Figure 17 for vertical strike-slip earthquakes. For rock sites, the standard deviation is independent of distance, but for soil sites, there is a strong distance dependence.
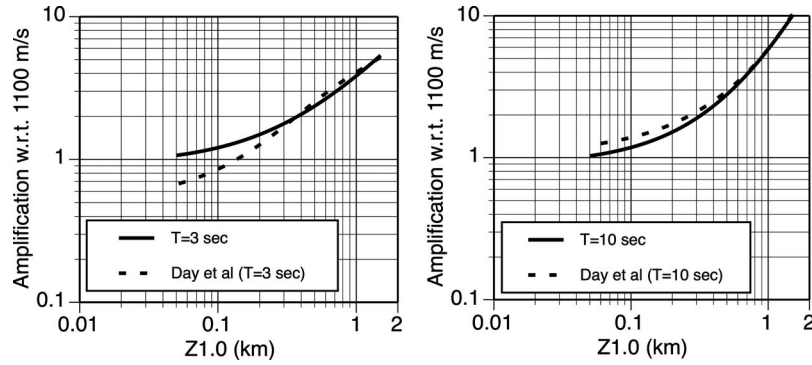
**Figure 15.** Comparison of the soil-depth scaling from the Day et al. (2006) 3-D basin response study with the net soil-depth scaling in our NGA model for T=3 sec and T=10 sec.

## APPLICATION GUIDELINES

### HANGING-WALL EFFECTS

The hanging-wall scaling was derived from only reverse faulting earthquakes. An issue is whether these HW factors are also applicable for normal faulting earthquakes. We believe that the HW factor is primarily a source-site geometry issue. Therefore, we recommend applying the HW factors to normal faulting earthquakes. We will revisit this recommendation as results from ongoing studies of hanging-wall effects for normal faults become available.
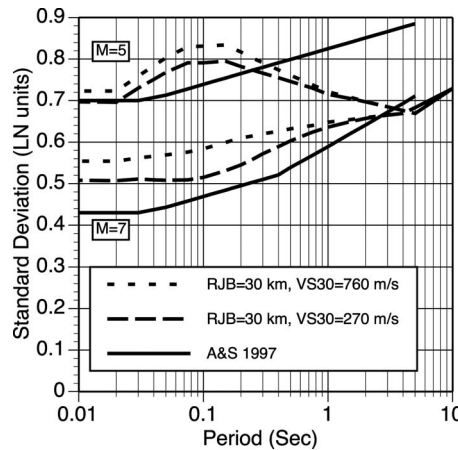


**Figure 16.** Comparison of the total standard deviation from the current model for $R_{JB}$=30 km with the standard deviation from the A&S (1997) model.
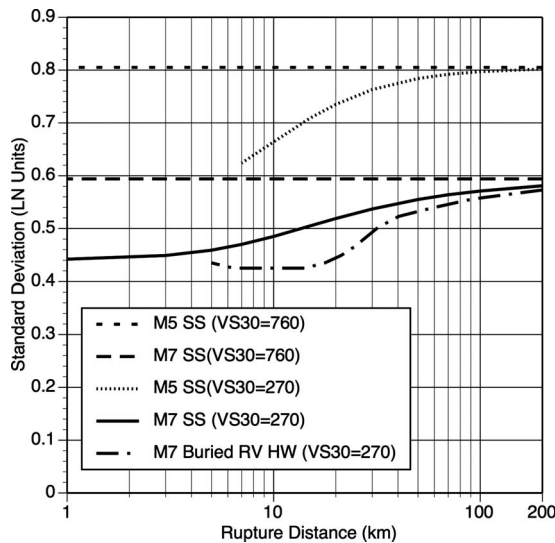
**Figure 17.** Distance dependence of the total standard deviation for T=0.2 sec spectral acceleration due to the nonlinear site response.

## DETERMINISTIC GROUND MOTIONS AND SOIL NON-LINEARITY

Our ground-motion model uses $PGA_{1100}$ to quantify the strength of shaking for the soil nonlinearity. Equation 4 uses the median $PGA_{1100}$. If a deterministic analysis is conducted for the 84th percentile ground motion, then it may seem that the 84th percentile $PGA_{1100}$ should be used in Equation 4, but that is not appropriate. The increased non-linearity for the 84th percentile $PGA_{1100}$ is already included in the standard deviation model. The median $PGA_{1100}$ should be used in our model even for deterministic analyses with above median ground motions.

## $V_{S30}$ AND THE STANDARD DEVIATION

Two models for the standard deviation are given: one if the $V_{S30}$ is measured at the site and one if the $V_{S30}$ is estimated. For our data set, the error in the $ln(V_{S30})$ is estimated to be 0.28 natural log units, on average. If the standard deviation model based on estimated $V_{S30}$ is used, then the standard deviation accommodates about 30% uncertainty in the $V_{S30}$. Therefore, it is not necessary to consider a range of $V_{S30}$ values if the $V_{S30}$ is accurate to within 30%. If the measured $V_{S30}$ standard deviation model is used, then the uncertainty in the measurement of $V_{S30}$ should be estimated by using a range of $V_{S30}$ values.

## SOIL DEPTH EFFECTS

The ground-motion model includes the depth to $V_S = 1.0$ km/s ($Z_{1.0}$) based on the analytical site response models. If this depth is not known, then the median $Z_{1.0}$ should be used based on Eq. 8. The standard deviation was derived without $Z_{1.0}$. Therefore, the standard deviation is applicable to the case in which $Z_{1.0}$ is not known. The intra-event standard deviation could be reduced if the $Z_{1.0}$ is known. At this time, we recommend using the standard deviations as listed in Table 4 until improved $Z_{1.0}$ values are available for the strong-motion sites.

## RANGE OF APPLICABILITY

Although the largest magnitude in the NGA data set is M7.9, we consider that the model can be reliably extrapolated to M8.5. The lower bound magnitude used in our data set is 4.27, but there are few data for the small magnitude range. Our model is focused on $M >= 5$ and we recommend not extrapolating below magnitude 5.0. For M5-8.5, the model is applicable to distances from 0 to 200 km.

## ACKNOWLEDGMENTS

## REFERENCES

Abrahamson, N. A., and Youngs, R. R., 1992. A stable algorithm for regression analyses using the random effects model, *Bull. Seismol. Soc. Am.* **82**, 505–510.

Abrahamson, N. A., and Silva, W., 1997. Empirical response spectral attenuation relations for shallow crustal earthquakes, *Seismol. Res. Lett.* **68**, 94–127.

Abrahamson, N. A., and Silva, W. J., 2008. *Abrahamson & Silva NGA ground motion relations for the geometric mean horizontal component of peak and spectral ground motion parameters*, Final report prepared for the Pacific Earthquake Engineering Research Center, February 2008.

Collins, N., Graves, R., and Somerville, P., 2006. *Revised analysis of 1-D rock simulations for the NGA-E project*, Final report prepared for the Pacific Earthquake Engineering Research Center, April 2006.

Day, S. M., Bielak, J., Dreger, D., Graves, R., Larsen, S., Olsen, K., and Pitarka, A., 2005. *3D ground motion simulations in basins*, Final report prepared for the Pacific Earthquake Engineering Research Center, Project 1A03.

Silva, W. J., 2005 *Site response simulations for the NGA project*, Report prepared for the Pacific Earthquake Engineering Research Center.

Somerville, P. G., and Pitarka, A., 2006. Differences in earthquake source and ground motion characteristics between surface and buried earthquakes, Proc. Eighth National Conf. Earthquake Engineering, Paper No, 977.

Walling, M., Silva, W. J., and Abrahamson, N. A., 2008. Nonlinear site amplification factors for constraining the NGA models, *Earthquake Spectra* **24**, 243–255.